Monthly Notices of the ROYAL ASTRONOMICAL SOCIETY

MNRAS **549,** 1–8 (2026)
Advance Access publication 2026 May 25

https://doi.org/10.1093/mnras/stag971

Nature of 4FGL J2249.4+6229: evidence for a redback system with a cool companion and low X-ray and γ-ray luminosities

A. V. Karpova [1], D. A. Zyuzin [1], S. V. Zharikov [2]★ and M. R. Gilfanov[3,4]

[1]*Ioffe Institute, Politekhnicheskaya 26, St. Petersburg 194021, Russia*
[2]*Instituto de Astronomía, Universidad Nacional Autónoma de México, Apdo. Postal 106, Baja California, Ensenada 22800, Mexico*
[3]*Space Research Institute of the Russian Academy of Sciences, Profsoyuznaya 84/32, Moscow 117997, Russia*
[4]*Max-Planck-Institut für Astrophysik, Karl-Schwarzschild-Str 1, D-85741 Garching, Germany*

Accepted 2026 May 19. Received 2026 May 5; in original form 2026 February 27

ABSTRACT

We report the identification of the likely X-ray and optical counterpart to the unassociated *Fermi* source 4FGL J2249.4+6229. To clarify its nature, we investigate the X-ray data from *Swift*/XRT and SRG/*eROSITA* as well as photometric data from optical catalogues and archival spectroscopic data from the *Gemini*-North telescope. Using Zwicky Transient Facility data spanning over 6.6 yr, we confirmed a period of ≈5.6 h likely associated with the orbital motion in a binary system. The folded light curves have a smooth sinusoidal shape with two peaks per period and the amplitude of ≈0.2 mag. The X-ray spectra of the source are well fitted by an absorbed power law with the photon index of ≈2.0 and unabsorbed flux of $\approx 1.4 \times 10^{-13}$ erg s^{-1} cm^{-2}. All these together with the X-ray to optical flux ratio of ∼0.2 implies that 4FGL J2249.4+6229 is a promising redback candidate. Fitting the optical light curves with the direct heating model, we obtained the companion mass of ≈0.5 $M_\odot$ and temperature of ≈3600 K implying an M-type star. This places it among the coldest and most massive companions known in redback systems. Optical spectra confirm the M-type star and show the broad asymmetric Hα emission line. For the distance of 500–550 pc derived from the optical data, the source can be the redback with the lowest X-ray and γ-ray luminosities.

Key words: binaries: close – stars: individual: 4FGL J2249.4+6229 – stars: neutron – X-rays: binaries.

1 INTRODUCTION

Thanks to the *Fermi Gamma-ray Space Telescope*, a large number of binary millisecond pulsars (MSPs) have been discovered in recent years. Among them, there are members of the 'spider' family: redbacks (RBs) and black widows (BWs) (M. S. E. Roberts 2013). They are characterized by short orbital periods, $P_b < 1$ d, and low-mass companion stars. Companions of BWs are semidegenerate and have masses $M_c < 0.05$ $M_\odot$, while RBs possess non-degenerate and more massive ($M_c \approx 0.1$–1 $M_\odot$) secondaries. Three RBs – the so-called transitional millisecond pulsars (tMSPs) – show transitions between rotation-powered pulsar and active X-ray states (A. Papitto & D. de Martino 2022) confirming the evolutionary link between low-mass X-ray binaries (LMXBs) and MSPs. The pulsar mass in spider systems can exceed 2 $M_\odot$ which makes their studies particularly important for constraining the equation of state of the superdense matter in neutron stars' (NSs) interiors (e.g. R. Kumar et al. 2023).

Spiders show orbital modulation in the optical due to the heating of the companion by the pulsar and/or its ellipsoidal shape (e.g. P. J. Callanan, J. van Paradijs & R. Rengelink 1995; P. Draghis et al. 2019; C. J. Clark et al. 2021; D. Kandel & R. W. Romani 2023; D. Mata Sánchez et al. 2023; O. G. Dodge et al. 2024), and in X-rays due to the intrabinary shock (IBS) produced by the interacting winds from the pulsar and its companion (e.g. R. W. Romani & N. Sanchez 2016; A. G. Sullivan & R. W. Romani 2024). The optical spectra are dominated by the cool secondary star (e.g. M. H. Kerkwijk, R. P. Breton & S. R. Kulkarni 2011; R. W. Romani & M. S. Shaw 2011; R. W. Romani, A. V. Filippenko & S. B. Cenko 2015; J. Strader et al. 2019; M. Turchetta et al. 2025), while the X-ray spectra are usually non-thermal and attributed to the IBS emission (e.g. S. R. Kulkarni et al. 1992; J. Arons & M. Tavani 1993; D. Kandel, R. W. Romani & H. An 2019; A. G. Sullivan & R. W. Romani 2025; A. G. Sullivan, J. T. Dinsmore & R. W. Romani 2026). However, a thermal component originating from the pulsar polar caps can also be present.

To date, about 80 confirmed spider pulsars have been detected in the Galactic field (K. I. I. Koljonen & M. Linares 2025). However, a significant challenge in detecting new spider pulsars via radio surveys is the periodic obscuration of the pulsar's radio emission by ablated material from the companion star, which prevents the detection of pulsations. Nevertheless, these systems can be identified through multiwavelength investigations, especially in the optical and X-rays, of likely counterparts to unassociated *Fermi* sources (e.g. D. Salvetti et al. 2017; C. Braglia et al. 2020). Currently, such studies have revealed about 30 spider candidates

★ E-mail: zhar@astro.unam.mx

(e.g. K.-L. Li et al. 2021; S. J. Swihart et al. 2021, 2022; J. P. Halpern 2022; A. V. Karpova et al. 2023, 2025; D. A. Zyuzin et al. 2024).

Here we report on the discovery of the likely X-ray and optical counterpart to the unassociated γ-ray source 4FGL J2249.4+6229 (hereafter J2249). According to the *Fermi* Large Area elescope 14-Year Point Source Catalog (4FGL-DR4; J. Ballet et al. 2023), its flux in the 0.1–100 GeV band is $F_\gamma \approx (9.98 \pm 1.84) \times 10^{-12}$ erg s^{-1} cm^{-2}. In addition, its steady emission and a spectrum, which can be described by the LogParabola model, suggest it could be a pulsar. Indeed, M. G. F. Mayer & W. Becker (2024) provided the probability of 0.92 for the source to be a pulsar rather than a blazar. We find that the properties of the J2249 presumed counterpart are typical for RB systems.

The X-ray and optical identification of the source is described in Section 2. Sections 3 and 4 contain the analysis of the data. The results and conclusions are given in Sections 5 and 6.

2 X-RAY/OPTICAL COUNTERPART IDENTIFICATION

To search for X-ray counterparts to J2249, we investigated X-ray data obtained in the course of five all-sky surveys in 2020–2022 with the extended ROentgen Survey with an Imaging Telescope Array (*eROSITA*) telescope (P. Predehl et al. 2021) aboard the Spectrum-RG (SRG) orbital observatory (R. Sunyaev et al. 2021). The J2249 field as observed by *eROSITA* is shown in Fig. 1, top. The brightest source within the γ-ray positional uncertainty ellipse, SRGe J224828.4+622210, is marked with the arrow. Its coordinates are $\alpha_X(2000) = 22^h48^m28^s.43$ and $\delta_X(2000) = +62^\circ22'10''.1$ and 90 per cent position uncertainty is 3.9 arcsec.

We also checked the Living *Swift*-XRT Point Source (LSXPS) catalogue (P. A. Evans et al. 2023). At the SRGe J224828.4+622210 position there is the source LSXPS J224828.5+622211 (Fig. 1, middle) with coordinates $\alpha_X(\mathrm{J2000}) = 22^h48^m28^s.57$ and $\delta_X(\mathrm{J2000}) = +62^\circ22'11''.7$ and 90 per cent position uncertainty 6.5 arcsec.

Then we examined the *Gaia* Data Release (DR) 3 catalogue (Gaia Collaboration 2016, 2023) and found a counterpart candidate to the X-ray source – *Gaia* DR3 2207925451446739072 with the magnitude $G \approx 18$ and effective temperature of about 3500 K. Its coordinates are $\alpha_{\mathrm{opt}}(\mathrm{J2016}) = 22^h48^m28^s.614$ and $\delta_{\mathrm{opt}}(\mathrm{J2016}) = +62^\circ22'11''.40$ and its proper motion is 12.3(1) mas yr^{-1}. The geometric and photogeometric distances to the source are similar, $D_{\mathrm{g}} = 525$–572 pc and $D_{\mathrm{pg}} = 537$–596 pc (C. A. L. Bailer-Jones et al. 2021). Thus, it definitely locates in the Galaxy. The interstellar absorption in this direction for the object distance is $E(B-V) = 0.30$–0.41 mag (G. M. Green et al. 2019).

The source is also presented in the Panoramic Survey Telescope and Rapid Response System survey (Pan-STARRS) DR 2 catalogue (H. A. Flewelling et al. 2020) where its designation is PSO J342.1192+62.3698. It remains the only counterpart candidate to SRGe J224828.4+622210 (see Fig. 1, bottom) even though the Pan-STARRS survey is deeper than the *Gaia* data. In addition, the source was found in the Zwicky Transient Facility (ZTF) catalogue of periodic variable stars (X. Chen et al. 2020) which is based on the DR 2 data covering approximately 1.3 yr. The source is listed as ZTF J224828.61+622211.4 and its period derived from the *r*-band light curve is 0.2334096 d. The *g*-band light curve gives a shorter period of 0.2090120 d, though the low significance makes this estimate unreliable.

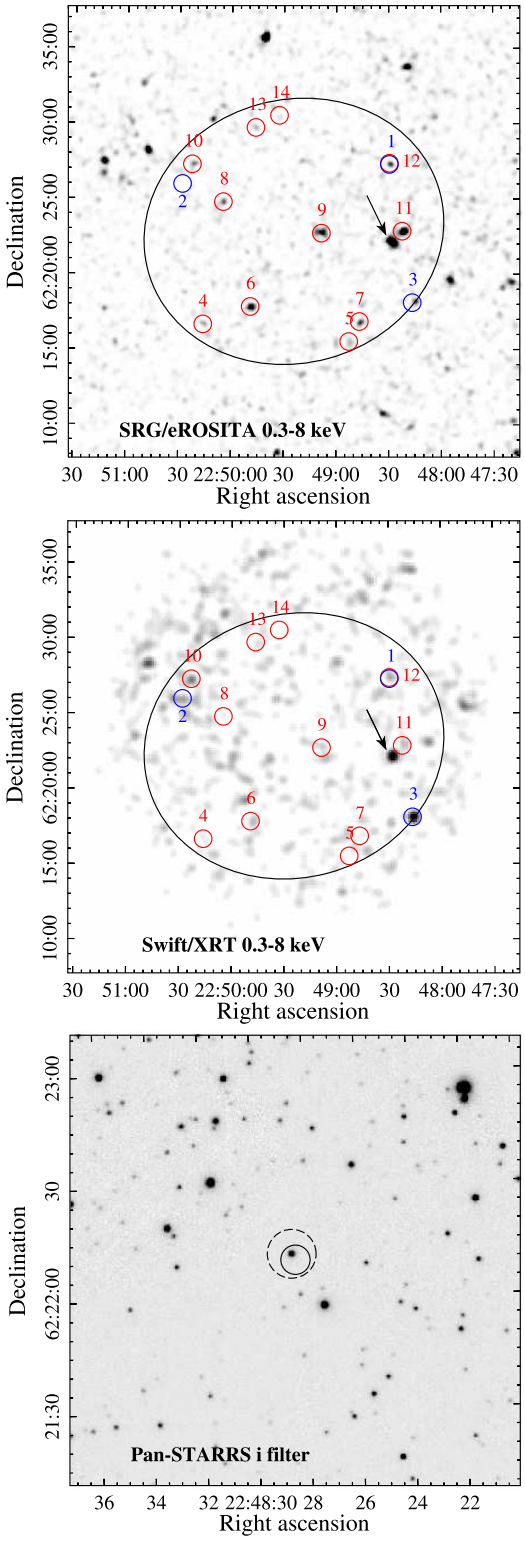

Figure 1. 30 × 30 arcmin^2 *eROSITA* (*top panel*) and *Swift* (*middle panel*) images in the 0.3–8 keV range. The ellipse shows the 95 per cent position uncertainty of the J2249 γ-ray position. The likely X-ray counterpart of J2249 is marked by the arrow. Other X-ray sources detected within the ellipse with *Swift* and *eROSITA* are shown by blue and red circles, respectively, and numbered. *Bottom*: 2 × 2 arcmin^2 Pan-STARRS image in the *i* band. The solid and dashed circles show the 90 per cent position uncertainties of the X-ray source obtained with *eROSITA* and *Swift*, respectively. The likely optical counterpart is seen inside the circles.

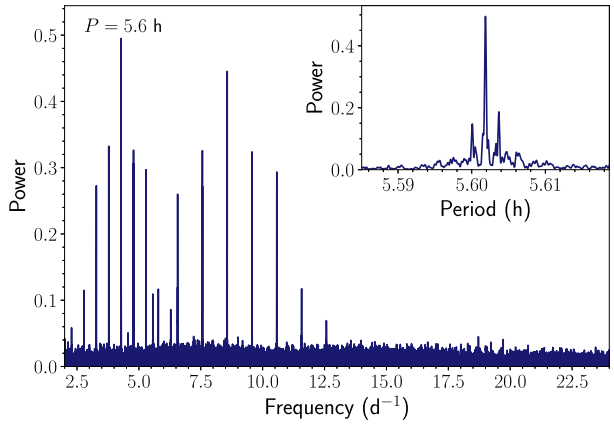

Figure 2. Lomb–Scargle periodogram of the J2249 optical counterpart candidate obtained using the *r*-band ZTF data and two harmonics. The best period $P = 5.6$ h corresponding to the highest peak is marked and the peak is enlarged in the inset.

3 OPTICAL DATA

3.1 Optical light curves and the orbital period

To check the period, we used the data from the ZTF DR 23 catalogue (F. J. Masci et al. 2019) which covers ≈6.6 yr and contains about 1000 measurements in the *r* band. We applied the NIFTY-LS Lomb–Scargle periodogram PYTHON package (L. H. Garrison et al. 2024) to them using one and two harmonics. The resulting power spectrum is shown in Fig. 2. The highest peak corresponds to the period,[1] $P = 0.2334112(57)$ d $= 5.60187(14)$ h.

We also checked the ZTF data in the *g* band, which contain about 650 measurements. We obtained the same best period [5.60186(14) h] although the corresponding power is significantly lower, mainly due to the high noise level of the data. Thus, the derived period is consistent with the value for the *r*-band data from the catalogue mentioned in Section 2.

The ZTF light curves in *g*, *r*, and *i* bands folded with the period *P* are shown in Fig. 3. They show two humps per period and one minimum is slightly deeper than the other.

3.2 Light curves modelling

To estimate the parameters of the presumed spider system, we fitted the folded light curves with the symmetric direct heating model. The details of the model can be found in S. Zharikov et al. (2013, 2019).

The model parameters are the distance to the binary system *D*, the reddening $E(B-V)$, the pulsar mass $M_{\rm NS}$, the mass ratio of the binary components *q*, the system orbit inclination *i*, the effective irradiation factor $K_{\rm irr}$ defining the companion heating, the companion Roche lobe filling factor *f*, and the companion 'night-side' temperature $T_{\rm n}$.

We fixed the orbital period at $P_{\rm orb} = 5.60187$ h. The effective 'night-side' temperature of the secondary, its irradiation, the Roche-lobe filling factor, the inclination, and the system mass ratio were initialized using a random sampling method. The initial

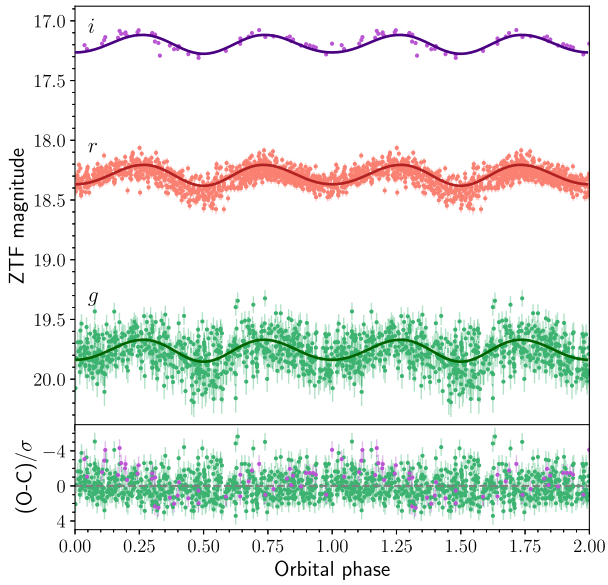

Figure 3. *Top*: ZTF light curves of the J2249 optical counterpart candidate in *g*, *r*, and *i* bands folded with the presumed orbital period of 5.60187 h. Two periods are shown for clarity. The best-fitting model is shown by the solid lines. The *r*-band light curve was excluded from the fitting (see text). The phase 0.0 is defined as the time when the secondary is placed between the pulsar and an observer. *Bottom*: Residuals derived for each data point as the difference between the observed (O) and the calculated (C) magnitudes divided by the error σ.

primary mass[2] was set to the canonical NS mass of 1.4 $M_\odot$, while initial values of the distance and interstellar extinction were randomly drawn from the ranges allowed by the *Gaia* and dust map (G. M. Green et al. 2019) estimates.

The minimum of the χ^2 function was determined using a gradient-descent algorithm, which was chosen because it substantially reduces the computational effort required for the minimization. The parameter uncertainties were calculated following the method proposed by M. Lampton, B. Margon & S. Bowyer (1976).

We found that the observed light curves can be reproduced without including irradiation of the secondary, i.e. $K_{\rm irr} = 0$ and $T_{\rm n} \equiv T_{\rm c}$, where $T_{\rm c}$ is the effective temperature of the companion. Furthermore, a pure blackbody approximation for the emission from the spider pulsar companions does not allow a simultaneous fit to all photometric bands. This is largely because the spectral energy distribution of cool companions deviates significantly from a blackbody, requiring more sophisticated atmosphere models to account for molecular absorption and other non-trivial atmospheric effects (see e.g. A. G. Sullivan & R. W. Romani 2024). Nevertheless, the best-fitting model reproduces the *g* and *i* bands well, but overestimates the flux in the *r* band. Therefore, only the *g* and *i* bands together were used to determine the best-fitting parameters, and the *r*-band model was subsequently adjusted by a constant magnitude offset ($\Delta r = +0.26$ mag), representing the flux difference between a blackbody and an M-dwarf atmosphere at the derived effective temperature.

[1]The period uncertainty was calculated as the half width at half maximum of the peak.

[2]The value serves as a starting guess for the optimization rather than a statistical prior.

Table 1. The light-curve fitting results for J2249.

Fitted parameters	
NS mass $M_{\rm NS}$, $M_\odot$	$1.53^{+0.05}_{-0.17}$
Mass ratio $q = M_{\rm c}/M_{\rm NS}$	0.35(3)
Distance D, pc	525(25)
Effective temperature $T_{\rm c}$, K	3560(50)
Inclination i, deg	50(30)
Roche lobe filling factor f_x	$1.00^{+0.00}_{-0.20}$
Reddening $E(B-V)$	0.35(5)
χ^2/d.o.f.	740/672
Derived parameters	
Companion mass $M_{\rm c}$, $M_\odot$	0.54
Companion radius $R^x_{\rm c}$, $R_\odot$	0.80
Companion radius $R^y_{\rm c}$, $R_\odot$	0.60

Note. Numbers in parentheses denote 1σ uncertainties related to the last significant digits. $R^x_{\rm c}$ and $R^y_{\rm c}$ are the radii of the ellipsoidal companion. The former is along the line passing through the centres of the binary sources. d.o.f. ≡ degrees of freedom.

The results of the fit are presented in Table 1, and the best-fitting models of the *g*-, *r*-, and *i*-band light curves are shown as solid lines in Fig. 3. The reported χ^2 is based on the *g* and *i* bands used for the minimization. Inclusion of the *r*-band data after the correction mentioned above results in χ^2/d.o.f. = 1435/1674. The upper limits on the primary mass and the mass ratio arise from the requirement that the Roche lobe radius of the secondary must not be smaller than the radius of a zero-age main-sequence star with a mass of $M_{\rm c} = q\,M_{\rm NS}$. For parameter values within these limits, the results are insensitive to the adopted initial conditions including starting mass of the pulsar.

3.3 Archival optical spectroscopy with *Gemini*

The optical spectral observations[3] of the J2249 counterpart candidate were performed with the *Gemini*-North telescope on 2022 June 10 and 22. Two long-slit spectra with 12-min exposures were obtained using the *Gemini* Multi-Object Spectrograph with the R400+_G5305 grating in conjunction with the GG455_G0305 longpass filter covering 4500–9300 Å. The slit width was 1″ and the resulting resolution was 8 Å at a blaze wavelength of 7640 Å.

Data reduction was performed using GEMINI reduction software based on the Image Reduction Analysis Facility (IRAF) package. To calibrate the flux, the spectra of the spectrophotometric standard EG13 were used.

Note, that both spectra of the J2249 likely counterpart were obtained approximately at the same orbital phase, $\phi \sim 0.3$. The resulting spectrum from June 10 is presented in Fig. 4. It was dereddened using the extinction law by E. L. Fitzpatrick (1999) and $E(B-V) = 0.35$ mag derived from the light-curve fitting. The continuum of spectrum corresponds to an usual M-type dwarf star but there are Balmer emission (H α and H β) lines too. The M2V-template[4] from A. Y. Kesseli et al. (2017) is also shown for comparison. The source spectrum is generally consistent with the template, although we note that there is a slight flux excess in the ∼5000–5600 Å range. The contribution of the excess in *g*-band light curve appears to be relatively weak and therefore not prominent in the rather noisy ZTF data.

The profiles of the H α emission line are shown in the insets of Fig. 4. The line is asymmetric, probably double-peaked, or has at least two distinct components. The red part of the profile is more intense than the blue one. The line has an equivalent width of $\mathrm{EW}_{\mathrm{H}\alpha} \approx -30$ Å and a full width at half-maximum of $\mathrm{FWHM}_{\mathrm{H}\alpha} \approx 20$ Å (or ∼900 km s^{-1}). We also fitted the line profile with the double-gaussian model. For both spectra, we obtained similar separation between the peak positions of the components of about 9 Å (or ∼400 km s^{-1}).

4 X-RAY SPECTRA

To study the X-ray spectrum of the J2249 counterpart candidate, we used SRG/*eROSITA* and archival *Swift*/XRT data. From the *eROSITA* data the source spectra were extracted using a circular region with a radius of 60 arcsec centred at the source position. For the background extraction, we used an annulus region with the inner and outer radii of 150 and 300 arcsec around the source. The background sources were excluded with 40 arcsec radius apertures,[5] 45.4 net counts were collected in the 0.3–9 keV band in the total exposure time of ≈2.7 ks (the vignetting corrected exposure is ≈1.4 ks).

The source was observed with *Swift* in 2019–2020 (ObsIDs 03110575001–03110575011) with the total exposure of ≈6.5 ks. The *Swift* spectrum was extracted utilizing the *Swift*-XRT data products generator[6] (P. A. Evans et al. 2009). This resulted in 15.7 net counts in the 0.3–10 keV band.

Both *eROSITA* and *Swift* spectra were grouped to ensure at least one count per energy bin and fitted with the X-Ray Spectral Fitting Package (XSPEC) v.12.15.0 (K. A. Arnaud 1996). The interstellar absorption was taken into account using the TBABS model with the WILM abundances (J. Wilms, A. Allen & R. McCray 2000).

The reddening $E(B-V) = 0.35$ obtained from the light-curve fitting was transformed to the absorbing column density $N_{\rm H} = 3 \times 10^{21}$ cm^{-2} utilizing the empirical relation from D. R. Foight et al. (2016). This value was fixed during the fitting procedure. The number of counts is low so we used the *C*-statistics (W. Cash 1979).

We applied the absorbed power-law (PL) model and found that the best-fitting parameters obtained for the *eROSITA* and *Swift* spectra are in agreement within their 1σ uncertainties. Thus, we fitted both spectra simultaneously which results in the photon index $\Gamma = 2.0^{+0.4}_{-0.3}$, the unabsorbed flux in the 0.5–10 keV band $F_{\rm X} = (1.4 \pm 0.3) \times 10^{-13}$ erg s^{-1} cm^{-2} and C/d.o.f. = 70/86. The spectra and the best-fitting model are presented in Fig. 5.

5 DISCUSSION

We have found a likely X-ray and optical counterpart to the unassociated *Fermi* source J2249. Its *Gaia* magnitude $G = 18.01$ and colour $BP - RP = 2.33$ combined with the observed X-ray flux in the 0.2–12 keV band of $\approx 1.2 \times 10^{-13}$ erg s^{-1} cm^{-2} provides the X-ray to optical flux ratio of ∼0.2. According to fig. 1 in A. C.

[3] PI S. Swihart, programme ID GN-2022A-Q-236

[4] The template can be found at https://svo2.cab.inta-csic.es/theory/newov/templates.php?model = tpl_kesseli

[5] Two sources were excluded from the background region and one (number 11 in Fig. 1) – from the source region.

[6] https://www.swift.ac.uk/user_objects/

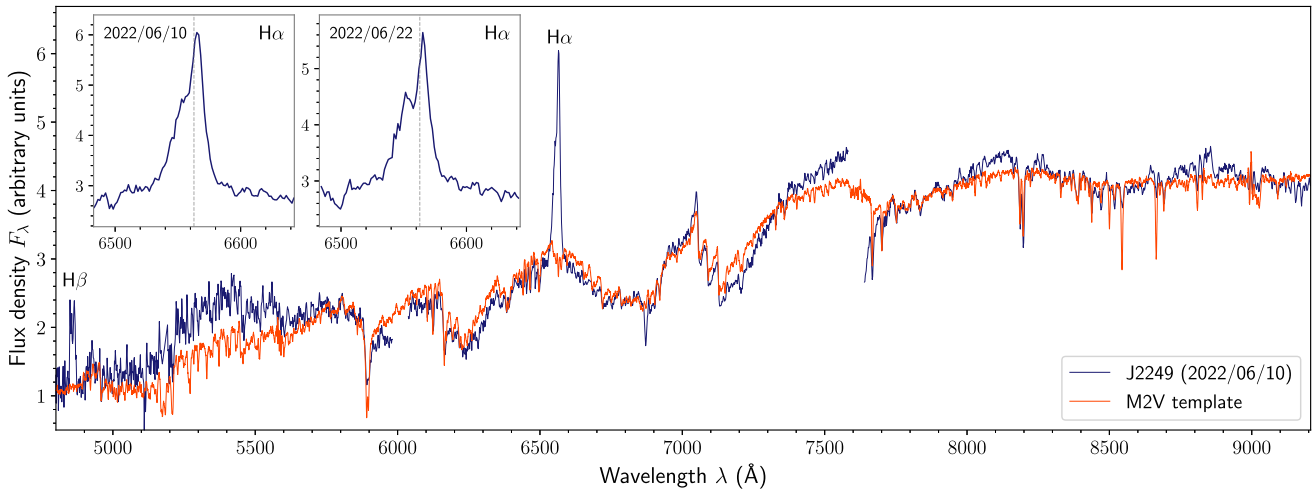

Figure 4. Dereddened optical spectrum of the likely J2249 counterpart (dark blue) obtained with the *Gemini*-North telescope on 2022 June 10 (the empty regions represent instrumental chip gaps). The orange line represents the M2-star template. Insets show the zoomed-in region around the Hα line from the spectra obtained on June 10 and 22. The rest wavelength (6562.8 Å) is marked by the dashed grey line.

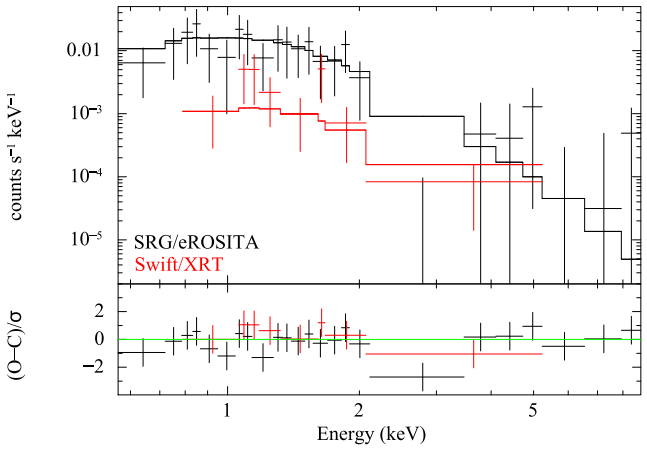

Figure 5. *Top*: the X-ray spectrum of the J2249 counterpart candidate with the best-fitting PL model. The data obtained by different instruments are marked by different colours as indicated in the panel. For illustrative purposes, the *eROSITA* and *Swift* spectra were grouped to ensure at least 3 and 2 counts per energy bin, respectively. *Bottom*: residuals derived for each data point as the difference between the observed (O) and the calculated (C) flux density divided by the error σ.

Rodriguez (2024), this implies that the source can belong to the spider pulsar family.

The optical light curves of the source are typical for RB systems where ellipsoidal modulations strongly dominate over the effect of the companion heating by the pulsar. Moreover, the irradiation effect here is small or even absent as observed for some RBs, e.g. PSR J1622−0315 or PSR J1816+4510 (K. I. I. Koljonen & M. Linares 2023; M. Turchetta et al. 2023).

The effective temperature of the J2249 counterpart candidate derived from the light-curve fitting is 3560(50) K which is close to the M2V-type star. This is confirmed by the optical spectroscopy. The flux excess in the ∼5000–5600 Å range, mentioned in Section 3.3, may be attributed to a hot spot on the companion's surface, as observed in some systems (e.g. S. J. Swihart et al. 2019; D. Kandel et al. 2020). However, additional time-resolved spectroscopic and photometric observations are needed to confirm its presence. Based on these results, J2249 can have one of the coldest companions among known RB systems. Indeed, typical temperatures are higher, about 4000–6000 K (e.g. M. Turchetta et al. 2023). The even lower base ('night-side') temperature of ≈3300 K was obtained only for PSR J2339−0533 (D. Kandel et al. 2020). In addition, PSR J1628−3205 can have a rather cold companion though its temperature is quite uncertain, 3560–4670 K (M. Li, J. P. Halpern & J. R. Thorstensen 2014).

With a mass of ≈0.5 $M_\odot$ the J2249 likely counterpart resides in the high-mass tail of the RB companion population (J. Strader et al. 2019), possibly making it one of the most massive known in this class. Other examples of massive sources are, e.g. companions of PSR J1306−4035 ($M_c = 0.51^{+0.02}_{-0.01}$ $M_\odot$; S. J. Swihart et al. 2019), PSR J1803−6707 ($M_c = 0.44^{+0.05}_{-0.04}$ $M_\odot$; A. Phosrisom et al. 2026), tMSP candidate 3FGL J0427.9−6704 [$M_c = 0.65(8)$; J. Strader et al. 2016], and RB candidate 1FGL J0523.5−2529 ($M_c \gtrsim 0.8$ $M_\odot$; J. Strader et al. 2014).

The most interesting feature in the optical spectrum of the J2249 likely counterpart is the Balmer emission lines. Such emission lines (sometimes clearly double peaked) were observed for some spider pulsars. For example, PSR J2339−0533 mentioned above shows strong Hα and weaker Hβ emission lines in some spectra (D. Kandel et al. 2020). Other examples are RBs PSR J1048+2339 (A. Miraval Zanon et al. 2021), PSR J1306−4035 (S. J. Swihart et al. 2019), PSR J1628−3205 (J. Strader et al. 2019), and PSR J0838−2827 (J. P. Halpern, J. Strader & M. Li 2017), RB candidate 1FGL J0523.5−2529 (J. P. Halpern, K. I. Perez & S. Bogdanov 2022), BW PSR J1311−3430 (R. W. Romani et al. 2015), BW candidates 4FGL J1408.6−2917 (S. J. Swihart et al. 2022), ZTF J1406+1222 (K. B. Burdge et al. 2022), and 4FGL J0935.3+0901 (Z. Wang et al. 2020; J. P. Halpern 2022). These sources also demonstrate flaring activity and variable heating. The emission lines are assumed to be associated with the IBS or with the companion wind/chromosphere. For the J2249 counterpart candidate, the broadness of the Hα line excludes its chromospheric origin (see B. Fuhrmeister et al. 2018) and allows one to associate it with the IBS.

The distance to the source obtained from the light curves modelling, 525(25) pc, agrees with the geometric and photogeometric values. For this distance, the proper motion $\mu = 12.3(1)$ mas yr^{-1} corresponds to the transverse velocity $v_t = 29$–32 km s^{-1} which is in compatible with velocities measured for binary pulsars (G. Hobbs et al. 2005). In addition, the best-fitting reddening agrees with the range, provided by the dust map of G. M. Green et al. (2019), 0.30–0.41 mag.

The source's X-ray luminosity in the 0.5–10 keV band is $L_X = (3.3\text{–}6.2) \times 10^{30}$ erg s^{-1} for 500–550 pc. This value is in agreement with the luminosity distribution for RBs, although it lies at the lower bound of the latter: only one RB PSR J1816+4510 has a similar low X-ray luminosity (K. I. I. Koljonen & M. Linares 2023). The γ-ray luminosity is $L_\gamma = (2.4\text{–}4.3) \times 10^{32}$ erg s^{-1}. This is also rather low for spider pulsars which typically have luminosities $> 10^{33}$ erg s^{-1} (K. I. I. Koljonen & M. Linares 2025).

The J2249 measured photon index $\Gamma = 2.0^{+0.3}_{-0.4}$ is consistent with the values observed for low-luminosity spider pulsars ($L_X \lesssim 10^{31}$ erg s^{-1}) while brighter RBs typically show harder non-thermal spectra (e.g. D. Kandel et al. 2019; A. G. Sullivan & R. W. Romani 2025). The softer emission in low-luminosity systems is likely attributed to a larger contribution from the heated polar caps relative to the IBS emission (K. I. I. Koljonen & M. Linares 2023).

By its X-ray to optical flux ratio, the J2249 presumed counterpart also agrees with accreting systems such as LMXBs or cataclysmic variables (CVs). However, the source has an overall harder X-ray spectrum than LMXBs in the low-luminosity regime ($L_X \lesssim 10^{32}$–10^{33} erg s^{-1}) when a thermal component from the bulk of the NS surface dominates (Y. Tanaka 1997). As for CVs with appropriate periods and donors, the interpretation cannot be fully ruled out. However, no strong flares or transition between low and high accretion states typical for many CV subclasses (K. Inight et al. 2023) are seen in the Pan-STARRS (MJD ≈55000–57000) and ZTF (MJD ≈58200–60600) data. The source is also stable in the *Gaia* data covering the time gap between Pan-STARRS and ZTF. The optical spectra show no evidence of the white dwarf emission (though it could be very cold) or bright accretion disc/flow suggesting a very low accretion rate. We could assume a low-accretion rate polar (e.g. A. D. Schwope 2025) but if so, the optical spectrum should exhibit pronounced cyclotron humps. Thus, if the source is indeed a CV, it represents a highly unique object with a low accretion rate that has remained stable for at least ∼15 yr. Moreover, it cannot be associated with the *Fermi* source.

We also investigated other X-ray sources marked in the top and middle panels of Fig. 1 as well as their possible optical counterparts. The details are presented in Appendix A. None of them seems to be responsible for the γ-ray emission.

6 CONCLUSIONS

To sum up, J2249 is likely a rare member of the RB family – one with a cool companion and unusually low X-ray and γ-ray luminosities. Such systems are challenging to detect due to the limited depth of current optical and X-ray surveys. At a distance just three times greater ($\gtrsim$1.5 kpc), J2249 would have remained undetected by *eROSITA* and *Swift*, and its optical periodicity would have been missed in ZTF data.

Searching for pulsations in the radio from an NS is needed to confirm the RB nature of the J2249 likely optical/X-ray counterpart. The present analysis is limited by the relatively noisy ZTF data and sparse spectroscopic coverage. Deeper, phase-resolved optical photometry and spectroscopy are therefore necessary to confirm and robustly constrain the system parameters, including the mass ratio and pulsar mass derived from radial velocity curves, and to investigate the IBS geometry.

ACKNOWLEDGEMENTS

We thank the anonymous referee for useful and constructive comments. This work has made use of data from the European Space Agency (ESA) mission *Gaia* (https://www.cosmos.esa.int/gaia), processed by the *Gaia* Data Processing and Analysis Consortium (DPAC, https://www.cosmos.esa.int/web/gaia/dpac/consortium). Funding for the DPAC has been provided by national institutions, in particular the institutions participating in the *Gaia* Multilateral Agreement. The Pan-STARRS1 Surveys (PS1) and the PS1 public science archive have been made possible through contributions by the Institute for Astronomy, the University of Hawaii, the Pan-STARRS Project Office, the Max-Planck Society and its participating institutes, the Max Planck Institute for Astronomy, Heidelberg and the Max Planck Institute for Extraterrestrial Physics, Garching, The Johns Hopkins University, Durham University, the University of Edinburgh, the Queen's University Belfast, the Harvard-Smithsonian Center for Astrophysics, the Las Cumbres Observatory Global Telescope Network Incorporated, the National Central University of Taiwan, the Space Telescope Science Institute, the National Aeronautics and Space Administration under Grant No. NNX08AR22G issued through the Planetary Science Division of the NASA Science Mission Directorate, the National Science Foundation Grant no. AST-1238877, the University of Maryland, Eotvos Lorand University (ELTE), the Los Alamos National Laboratory, and the Gordon and Betty Moore Foundation. Based on observations obtained with the Samuel Oschin Telescope 48-inch and the 60-inch Telescope at the Palomar Observatory as part of the *Zwicky* Transient Facility project. ZTF was supported by the National Science Foundation under Grant Nos AST-1440341 and AST-2034437 and a collaboration including current partners Caltech, IPAC, the Oskar Klein Center at Stockholm University, the University of Maryland, University of California, Berkeley, the University of Wisconsin at Milwaukee, University of Warwick, Ruhr University, Cornell University, Northwestern University, and Drexel University. Operations are conducted by COO, IPAC, and UW. This work made use of data supplied by the UK Swift Science Data Centre at the University of Leicester. This work used data obtained with eROSITA telescope onboard SRG observatory. The SRG observatory was built by Roskosmos in the interests of the Russian Academy of Sciences represented by its Space Research Institute (IKI) in the framework of the Russian Federal Space Program, with the participation of the Deutsches Zentrum für Luft- und Raumfahrt (DLR). The SRG/eROSITA X-ray telescope was built by a consortium of German Institutes led by MPE, and supported by DLR. The SRG spacecraft was designed, built, launched, and is operated by the Lavochkin Association and its subcontractors. The science data are downlinked via the Deep Space Network Antennae in Bear Lakes, Ussurijsk, and Baykonur, funded by Roskosmos. The eROSITA data used in this work were processed using the eSASS software system developed by the German eROSITA consortium and proprietary data reduction and analysis software developed by the Russian eROSITA Consortium. The work of AVK and DAZ (periodicity search, reduction of the *Gemini* data, investigation of X-ray sources in the *Fermi* ellipse)

was supported by the baseline project FFUG-2024-0002 of the Ioffe Institute. The analysis of the J2249 X-ray spectra by AVK was supported by the Russian Science Foundation project 22-12-00048-P. DAZ thanks Pirinem School of Theoretical Physics for hospitality. SVZ acknowledges DGAPA-PAPIIT grant IN105826.

DATA AVAILABILITY

The ZTF data are available through the archive https://irsa.ipac.caltech.edu/Missions/ztf.html, *Swift*/XRT data – https://www.swift.ac.uk and eROSITA data – on request.

REFERENCES

Arnaud K. A., 1996, in Jacoby G. H., Barnes J., eds, ASP Conf. Ser. Vol. 101, Astronomical Data Analysis Software and Systems V. Astron. Soc. Pac., San Francisco, p. 17
Arons J., Tavani M., 1993, ApJ, 403, 249
Bailer-Jones C. A. L., Rybizki J., Fouesneau M., Demleitner M., Andrae R., 2021, AJ, 161, 147
Ballet J., Bruel P., Burnett T. H., Lott B., The Fermi-LAT collaboration, 2023, preprint (arXiv:2307.12546)
Braglia C. et al., 2020, MNRAS, 497, 5364
Burdge K. B. et al., 2022, Nature, 605, 41
Callanan P. J., van Paradijs J., Rengelink R., 1995, ApJ, 439, 928
Cash W., 1979, ApJ, 228, 939
Chen X., Wang S., Deng L., de Grijs R., Yang M., Tian H., 2020, ApJS, 249, 18
Clark C. J. et al., 2021, MNRAS, 502, 915
Dodge O. G. et al., 2024, MNRAS, 528, 4337
Draghis P., Romani R. W., Filippenko A. V., Brink T. G., Zheng W., Halpern J. P., Camilo F., 2019, ApJ, 883, 108
Evans P. A. et al., 2009, MNRAS, 397, 1177
Evans P. A., Page K. L., Beardmore A. P., Eyles-Ferris R. A. J., Osborne J. P., Campana S., Kennea J. A., Cenko S. B., 2023, MNRAS, 518, 174
Fitzpatrick E. L., 1999, PASP, 111, 63
Flewelling H. A. et al., 2020, ApJS, 251, 7
Foight D. R., Güver T., Özel F., Slane P. O., 2016, ApJ, 826, 66
Fuhrmeister B. et al., 2018, A&A, 615, A14
Gaia Collaboration, 2016, A&A, 595, A1
Gaia Collaboration, 2023, A&A, 674, A1
Garrison L. H., Foreman-Mackey D., Shih Y.-h., Barnett A., 2024, Res. Notes Am. Astron. Soc., 8, 250
Green G. M., Schlafly E., Zucker C., Speagle J. S., Finkbeiner D., 2019, ApJ, 887, 93
Halpern J. P., 2022, ApJ, 932, L8
Halpern J. P., Strader J., Li M., 2017, ApJ, 844, 150
Halpern J. P., Perez K. I., Bogdanov S., 2022, ApJ, 935, 151
Hobbs G., Lorimer D. R., Lyne A. G., Kramer M., 2005, MNRAS, 360, 974
Inight K. et al., 2023, MNRAS, 524, 4867
Kandel D., Romani R. W., 2023, ApJ, 942, 6
Kandel D., Romani R. W., An H., 2019, ApJ, 879, 73
Kandel D., Romani R. W., Filippenko A. V., Brink T. G., Zheng W., 2020, ApJ, 903, 39
Karpova A. V., Zyuzin D. A., Shibanov Y. A., Gilfanov M. R., 2023, MNRAS, 524, 3020
Karpova A. V., Zharikov S. V., Zyuzin D. A., Kirichenko A. Y., Shibanov Y. A., Márquez I. F., 2025, A&A, 693, A158
Kesseli A. Y., West A. A., Veyette M., Harrison B., Feldman D., Bochanski J. J., 2017, ApJS, 230, 16
Koljonen K. I. I., Linares M., 2023, MNRAS, 525, 3963
Koljonen K. I. I., Linares M., 2025, ApJ, 994, 8
Kulkarni S. R., Phinney E. S., Evans C. R., Hasinger G., 1992, Nature, 359, 300
Kumar R., Kumar M., Thakur V., Kumar S., Kumar P., Sharma A., Agrawal B. K., Dhiman S. K., 2023, Phys. Rev. C, 107, 055805
Lampton M., Margon B., Bowyer S., 1976, ApJ, 208, 177
Li K.-L., Jane Yap Y. X., Hui C. Y., Kong A. K. H., 2021, ApJ, 911, 92
Li M., Halpern J. P., Thorstensen J. R., 2014, ApJ, 795, 115
Masci F. J. et al., 2019, PASP, 131, 018003
Mata Sánchez D. et al., 2023, MNRAS, 520, 2217
Mayer M. G. F., Becker W., 2024, A&A, 684, A208
Miraval Zanon A. et al., 2021, A&A, 649, A120
Papitto A., de Martino D., 2022, in Bhattacharyya S., Papitto A., Bhattacharya D., eds, Astrophysics and Space Science Library, Vol. 465, Springer International Publishing, Springer Nature, Switzerland AG, p. 157
Phosrisom A. et al., 2026, MNRAS, 545, staf2173
Predehl P. et al., 2021, A&A, 647, A1
Roberts M. S. E., 2013, in van Leeuwen J. ed., Proc. IAU Symp. 291, Neutron Stars and Pulsars: Challenges and Opportunities after 80 years. Kluwer, Dordrecht, p. 127,
Rodriguez A. C., 2024, PASP, 136, 054201
Romani R. W., Sanchez N., 2016, ApJ, 828, 7
Romani R. W., Shaw M. S., 2011, ApJ, 743, L26
Romani R. W., Filippenko A. V., Cenko S. B., 2015, ApJ, 804, 115
Salvetti D. et al., 2017, MNRAS, 470, 466
Schwope A. D., 2025, A&A, 698, A106
Strader J., Chomiuk L., Sonbas E., Sokolovsky K., Sand D. J., Moskvitin A. S., Cheung C. C., 2014, ApJ, 788, L27
Strader J., Li K.-L., Chomiuk L., Heinke C. O., Udalski A., Peacock M., Shishkovsky L., Tremou E., 2016, ApJ, 831, 89
Strader J. et al., 2019, ApJ, 872, 42
Sullivan A. G., Romani R. W., 2024, ApJ, 974, 315
Sullivan A. G., Romani R. W., 2025, ApJ, 984, 146
Sullivan A. G., Dinsmore J. T., Romani R. W., 2026, ApJ, 999, 128
Sunyaev R. et al., 2021, A&A, 656, A132
Swihart S. J., Strader J., Chomiuk L., Shishkovsky L., 2019, ApJ, 876, 8
Swihart S. J., Strader J., Aydi E., Chomiuk L., Dage K. C., Shishkovsky L., 2021, ApJ, 909, 185
Swihart S. J., Strader J., Chomiuk L., Aydi E., Sokolovsky K. V., Ray P. S., Kerr M., 2022, ApJ, 941, 199
Tanaka Y., 1997, in Meyer-Hofmeister E., Spruit H., eds, Accretion Disks – New Aspects, Vol. 487. Springer, Germany, p. 1
Turchetta M., Linares M., Koljonen K., Sen B., 2023, MNRAS, 525, 2565
Turchetta M., Sen B., Simpson J. A., Linares M., Breton R. P., Casares J., Kennedy M. R., Shahbaz T., 2025, MNRAS, 538, 380
van Kerkwijk M. H., Breton R. P., Kulkarni S. R., 2011, ApJ, 728, 95
Wang Z. et al., 2020, MNRAS, 493, 4845
Wilms J., Allen A., McCray R., 2000, ApJ, 542, 914
Zharikov S., Tovmassian G., Aviles A., Michel R., Gonzalez-Buitrago D., García-Díaz M. T., 2013, A&A, 549, A77
Zharikov S., Kirichenko A., Zyuzin D., Shibanov Y., Deneva J. S., 2019, MNRAS, 489, 5547
Zyuzin D. A., Kirichenko A. Y., Karpova A. V., Shibanov Y. A., Zharikov S. V., Gilfanov M. R., Perez Tórtola C., 2024, MNRAS, 527, 6712

APPENDIX A: OTHER X-RAY SOURCES IN THE 4FGL J2249.4+6229 POSITION UNCERTAINTY ELLIPSE AND THEIR POSSIBLE OPTICAL COUNTERPARTS

Table A1 presents X-ray sources found inside the 4FGL J2249.4+6229 95 per cent position uncertainty ellipse, with the exception of the RB candidate. They are numbered as in the top and middle panels of Fig. 1. We note, that sources 2 and 3 were not detected with *eROSITA* that indicates their rather strong variability in X-rays, possibly flaring activity. Other sources are too weak to make any definitive conclusions about their variability.

To clarify the nature of the sources, we also searched for their likely optical counterparts in the *Gaia* catalogue and estimated

Table A1. X-ray sources in the 4FGL J2249.4+6229 position uncertainty ellipse and their likely optical counterparts.

Err_{90}	α_{opt}, δ_{opt}	f_X/f_{opt}	$BP-RP$	Comments
	(1) LSXPS J224829.5+622718/ (12) SRGe J224829.6+622723			
7.8	$22^h48^m28^s.69$, $+62°27'25''.2$	0.03	1.95	F-type star
	(2) LSXPS J225028.2+622559 – variable in X-rays			
6.4	(A) $22^h50^m27^s.99$, $+62°26'00''.7$	0.2	3.30	Late-type star, likely counterpart to the X-ray source
	(B) $22^h50^m28^s.19$, $+62°26'02''.5$	0.8	2.15	Late-type star
	(3) LSXPS J224816.5 + 6218 – variable in X-rays			
5.8	$22^h48^m16^s.20$, $+62°18'09''.2$	0.08	2.57	RS CVn, $P_b \approx 2.3$ d (X. Chen et al. 2020)
	(4) SRGe J225016.1+621641			
7.8	$22^h50^m15^s.72$, $+62°16'47''.0$	0.1	3.34	Late-type star
	(5) SRGe J224852.8+621533			
9.7	$22^h48^m53^s.24$, $+62°15'28''.2$	0.02	3.35	YSO (Gaia Collaboration 2023)
	(6) SRGe J224949.1+621751			
7.3	$22^h49^m48^s.55$, $+62°17'49''.6$	0.006	2.34	Active F-type star
	(7) SRGe J224846.8+621653			
6.9	$22^h48^m46^s.01$, $+62°16'54''.8$	0.08	3.23	Late-type star, likely YSO
	(8) SRGe J225004.8+622448			
7.1	$22^h50^m04^s.76$, $+62°24'54''.5$	0.002	1.71	Active G-type star, likely binary
	(9) SRGe J224908.5+622244			
7.4	$22^h49^m08^s.56$, $+62°22'45''.8$	0.01	2.42	RS CVn, $P_b \approx 1.8$ d (X. Chen et al. 2020)
	(10) SRGe J225022.7+622718			
9.7	$22^h50^m22^s.54$, $+62°27'20''.9$	0.006	2.38	YSO (Gaia Collaboration 2023)
	(11) SRGe J224822.3+622253			
5.2	$22^h48^m21^s.82$, $+62°22'54''.3$	0.006	1.90	Active late-type star
	(13) SRGe J224946.3+622945			
8.9	$22^h49^m46^s.82$, $+62°29'48''.9$	0.03	3.54	YSO (Gaia Collaboration 2023)
	(14) SRGe J224932.8+623033			
8.7	$22^h49^m32^s.11$, $+62°30'30''.5$	0.03	3.22	YSO (Gaia Collaboration 2023)

Note. Err_{90} is the 90 per cent position uncertainty of the X-ray source measured in arcsec; if the source is presented in both *Swift* and *eROSITA* data, the more precise position was used. α_{opt} and δ_{opt} are coordinates of the possible *Gaia* counterparts. f_X is the observed X-ray flux in the 0.2–12 keV band. f_{opt} is the observed optical flux calculated using the *G*-band magnitude. RS CVn: RS Canum Venaticorum-type binary system, YSO: young stellar object.

X-ray to optical flux ratios f_X/f_{opt}. Observed X-ray fluxes were calculated from the mean count rates using the WebPIMMS tool[7] and assuming the absorbed PL model with the column density $N_H = 3 \times 10^{20}$ cm^{-2} and photon index $\Gamma = 2$. Observed optical fluxes were obtained from the *Gaia* magnitude *G*. If several optical sources coincide with the X-ray source, f_X/f_{opt} should be considered as an upper limit.

We also used information from the Pan-STARRS and ZTF catalogues as well as optical-infrared spectral energy distributions (SEDs) of the sources[8] and distance estimates from C. A. L. Bailer-Jones et al. (2021) to establish the most probable nature of the sources, which is mentioned in Table A1. Note, that we present only the most plausible optical counterpart for each X-ray source. If no compelling candidate is found, all optical sources within the X-ray positional error circle are reported.

This paper has been typeset from a TEX/LATEX file prepared by the author.

[7] https://heasarc.gsfc.nasa.gov/cgi-bin/Tools/w3pimms/w3pimms.pl

[8] SEDs were obtained through the VizieR Photometry viewer https://vizier.cds.unistra.fr/vizier/sed/